THE JOURNAL OF PHYSICAL CHEMISTRY Letters

pubs.acs.org/JPCL Letter

# Variable Membrane Dielectric Polarization Characteristic in Individual Live Cells

Insu Park,[@] Jong Won Lim,[@] Sung Hoon Kim,[@] Seungyeop Choi, Kwan Hwi Ko, Myung Gu Son, Woo-Jin Chang, Young Ro Yoon, Sejung Yang, Jaehong Key, Yoon Suk Kim, Kilho Eom, Rashid Bashir, Sei Young Lee,* and Sang Woo Lee*

Cite This: *J. Phys. Chem. Lett.* 2020, 11, 7197−7203 Read Online

ACCESS | Metrics & More | Article Recommendations | Supporting Information

**ABSTRACT:** Investigation of the dielectric properties of cell membranes plays an important role in understanding the biological activities that sustain cellular life and realize cellular functionalities. Herein, the variable dielectric polarization characteristics of cell membranes are reported. In controlling the dielectric polarization of a cell using dielectrophoresis force spectroscopy, different cellular crossover frequencies were observed by modulating both the direction and sweep rate of the frequency. The crossover frequencies were used for the extraction of the variable capacitance, which is involved in the dielectric polarization across the cell membranes. In addition, this variable phenomenon was investigated by examining cells whose membranes were cholesterol-depleted with methyl-$\beta$-cyclodextrin, which verified a strong correlation between the variable dielectric polarization characteristics and membrane composition changes. This study presented the dielectric polarization properties in live cells' membranes that can be modified by the regulation of external stimuli and provided a powerful platform to explore cellular membrane dielectric polarization.

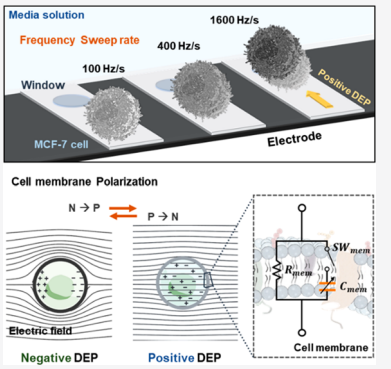




The dielectric polarization property of live cells has been employed in many biological activities that sustain life. For example, the cellular membrane capacitor in a neuron, which is determined by the dielectric polarization property that is in turn controlled by transmembrane ion flow, generates the neuronal potential needed to transfer an electrical signal.[1−3] The potential across a cellular membrane capacitor also regulates ion channels, transports, pumps, and enzymes.[4] When endocytosis or exocytosis occurs, the capacitance of the membrane capacitor changes.[5] Recent advances in bionanotechnology have enabled the measurement of electric potential in individual cell membranes (e.g., nanopillar-shaped electrode arrays,[6,7] nanoscale field-effect transistors embedded in bioprobes,[8] microscale or nanoscale pipet patch-clamping[9,10]).Through the combination of those potentials with a resistance-capacitance circuit model, deep investigation of the ion channel, transporters, and the transmission of electrical signals at the single-cell level can be achieved.[4,6,9] Therefore, to understand the functionalities of bioelectrical membrane that is necessary to maintain cellular life, the characterization of the dielectric polarization properties is essential. Recently, nonlinear dielectric polarization characteristics in a live cell were reported: the dielectrophoretic (DEP) phenomenon occurred through an interaction between the dielectric polarization property of a cell membrane and an external nonuniform electrical signal.[11] For instance, when electrical signals with different frequency modulation rates were applied to a cellular system, the cells moved with different velocities, even in the same frequency range.[12] In another example, a signal with different frequency modulation directions also induced different cellular velocities and crossover frequencies.[13] That is, cellular dielectric polarization is a function of the frequency modulation rate and direction, which indicates that the membrane capacitor of an individual live cell can possess variable capacitance with respect to an external electrical signal. However, no study has reported such a variable membrane dielectric characteristic, which is distinguished from the characteristics of static dielectric polarization already reported,[1−4,9] despite of its importance in understanding cellular functionalities.

Therefore, we used microfluidic DEP force spectroscopy (MDFS) to control the dielectric polarization of microscale particles (and the buffer solution surrounding those particles) during their interaction with a nonuniform electric field induced by AC input signals.[14−16] This method can also conveniently and noninvasively manipulate many individual live cells at the same time through DEP force, which is modulated by varying the frequency of the AC signals.[17−19] Furthermore, the frequency can be increased or decreased at

**Received:** May 10, 2020
**Accepted:** August 9, 2020




https://dx.doi.org/10.1021/acs.jpclett.0c01427
*J. Phys. Chem. Lett.* 2020, 11, 7197−7203

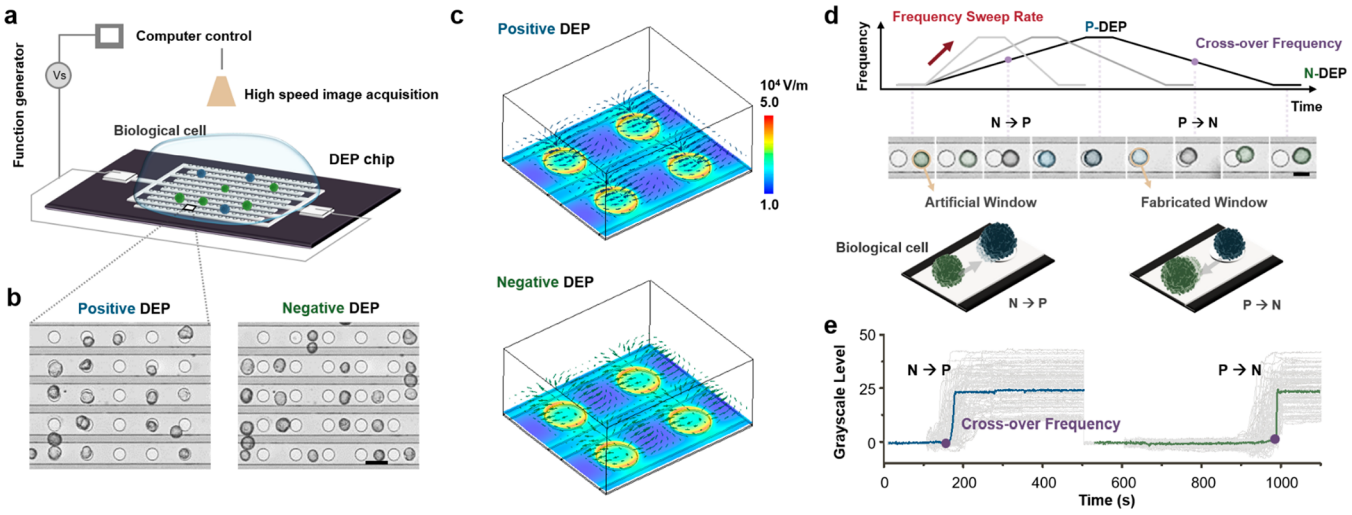


**Figure 1.** Microfluidic DEP force spectroscopy system for the observation of cellular movement. (a), Schematic illustration of the microfluidic DEP force spectroscopy system. (b) Optical images of the interdigitated electrode illustrating the positive and negative DEP forces that act on the cells. Scale bar, 30 $\mu$m. (c) Numerical simulation results from the positive DEP and negative DEP regions of (b) representing the force vectors and electric field gradient. (d) N → P and P → N frequency modulations of the AC input signal in combination with the frequency sweep rate and *in situ* monitoring of the resulting cell movements. The cell was trapped and released from the trap window by the DEP force of those modulations. Scale bar, 15 $\mu$m. (e) Variations in the grayscale level while a cell trapped in an artificial window by negative DEP force was being released during N → P modulation and the reverse case. The $f_{\text{co-effective}}$ in the graph of the grayscale level is the frequency at which the trapped cell starts to move from the trap position (e.g., artificial window during N → P modulation and fabricated window during P → N modulation).

will while maintaining homogeneous experimental conditions. (In the present context, "N → P" and "P → N" frequency modulations represent the application of two distinct input signals, where N and P stand for negative DEP force and positive DEP force, respectively.) Thus, the MDFS experiments allowed us to directly observe the dynamic dielectric polarization characteristics of live cells. In that way, we simultaneously measured the effective crossover frequencies, at which negative DEP force instantaneously changes into positive DEP force or vice versa, of many MCF-7 live cells while manipulating the DEP force by modulating its frequency, frequency sweep rates, and direction. We found different crossover frequencies and identical crossover frequencies in the live cells when the frequency changed in the N → P and P → N directions, respectively. This distinct characteristic indicates that the cellular membrane has a variable dielectric polarization property in its response to an external electrical signal and that it can be varied as a function of the frequency direction and sweep rate modulation. To investigate the characteristic more clearly, we also examined variable dielectric polarization properties from MCF-7 cells with depleted membrane cholesterol and from different types of cells (HeLa and A549 cells). We found a strong correlation between the variable dielectric polarization property and cellular membrane composition in live cells.

First, to observe a cellular behavior under frequency modulation, we introduced MCF-7 human breast cancer cells, whose biophysical and biochemical properties have been previously characterized into an MDFS system consisting of an interdigitated electrode array covered by a thin silicon dioxide layer containing circular trap windows.[20] A nonuniform electric field was then generated by applying an AC signal, which led to the dielectric polarization of both the individual MCF-7 cells and the surrounding buffer (Figure 1a,b). Theoretically, those dielectric polarizations, and hence the resulting DEP forces, are frequency-dependent.[21,22] The force vectors in the positive and negative DEP forces acting on the cells depicted in Figure 1b were also demonstrated using the finite-element method (COMSOL Multiphysics, 3.5a) in Figure 1c and Figure S4. In our experiment, the DEP force made individual cells move toward the circular window region as the frequency increased from 1 kHz to 41 kHz (N → P modulation), and it moved them toward the midpoint between adjacent windows when the frequency varied in the opposite (P → N) direction (Figure 1d, Method). In the N → P modulation region, the membrane polarization increased, producing cellular movement toward the region of the highest electric-field gradient, which in our device was inside the trap windows. In contrast, when the membrane polarization decreased, the cells moved toward the regions with the lowest electric-field gradient, located at the midpoints between the windows (Supporting Information S4 and S5).[22] Moreover, the frequency at which a cell's behavior changed instantly (e.g., the frequency at the moment that a cell, as shown in Figure 1d, moved out of the artificial windows during N → P modulation or the fabricated windows during P → N modulation) can be measured in a single condition (sequentially during N → P modulation and P → N modulation or sequentially vice versa). This measurement of a cell's behavior indicates that negative DEP force acting on a cell in the artificial window changes instantly into positive DEP force (or vice versa) during the modulations we induced. Therefore, the effective crossover frequency ($f_{\text{co-effective}}$) was defined as the measured frequency at which cellular behavior was instantaneously changed (Figure 1e, Supporting Information S7). Put another way, the measured $f_{\text{co-effective}}$ approximates the crossover frequency at which DEP force becomes zero (i.e., $F_{\text{DEP}} = 0$) in our measurement system.

Next, to investigate the membrane dielectric polarization property with respect to the frequency modulation, we measured the $f_{\text{co-effective}}$ of more than 150 cells simultaneously during both N → P and P → N modulations in combination with various frequency sweep rates (FSRs) under the same


https://dx.doi.org/10.1021/acs.jpclett.0c01427
J. Phys. Chem. Lett. 2020, 11, 7197−7203

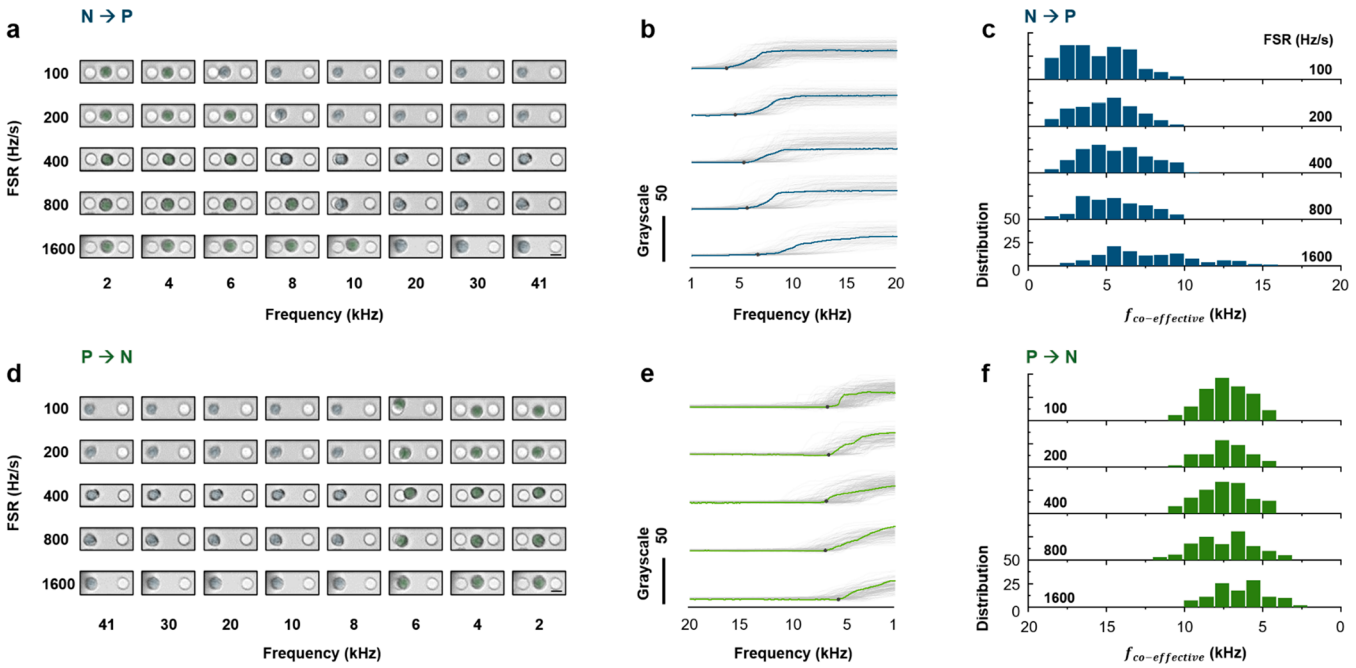


**Figure 2.** Measuring the $f_{co\text{-}effective}$ for both N → P and P → N modulation at various FSRs. (a) (b) Time sequential images showing the translational movement of the cells during N → P modulation (a) and P → N modulation (d) at 100−1600 Hz/s. Scale bar, 15 $\mu$m. (b), (e) Variation in grayscale level while cells trapped in an artificial window by negative DEP force were being released during N → P modulation (b) and vice versa (e). The blue and green lines indicate the specific grayscale values in (a) and (d), respectively. (c), (f) Histograms of the $f_{co\text{-}effective}$ of MCF-7 cells as a function of the frequency during N → P (c) and P → N (f) modulation.

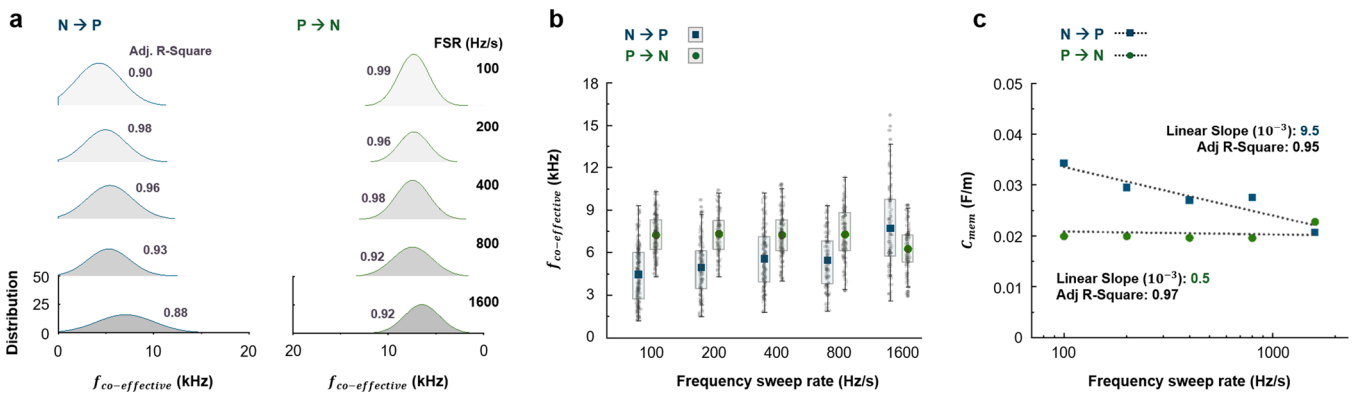


**Figure 3.** Variable dielectric polarization characteristic of MCF-7 cells at various FSRs. (a) Gaussian distribution functions of $f_{co\text{-}effective}$ derived from the measurement histogram data for N → P and P → N modulation, respectively. (b) Average and standard deviation of the Gaussian distributions, $f_{co}$. (c) Membrane capacitances during N → P and P → N modulation, respectively. The statistical reliability of the data in (b) and the measurement consistency of $f_{co}$ with 610 cells are provided in Supporting Information S14 and S17, respectively.

conditions, as shown in Figure 2. Time sequential images captured at 20 frames per second depict the change in the trapped positions of individual cells at different FSR conditions (100, 200, 400, 800, 1600 Hz/s) as the input frequency increases (N → P modulation) and decreases (P → N modulation) (Figure 2a,d). To measure $f_{co\text{-}effective}$, the grayscale levels from the time sequential images were measured for each FSR condition. Thus, $f_{co\text{-}effective}$ was determined using measurement data at the time when cells trapped in the artificial windows by negative DEP force were being released during N → P modulations and vice versa (Figure 2b,e). The histograms of $f_{co\text{-}effective}$ shown in Figure 2c,f reflect the grayscale level measurement of more than 150 cells in a single experimental condition during N → P and P → N modulation at FSRs of 100−1600 Hz/s. Interestingly, the overall distribution of $f_{co\text{-}effective}$ for N → P modulation shifted toward a higher frequency range as the FSR increased, whereas the distribution did not shifted regardless of the FSR during P → N modulation. Thus, the characteristic features of dielectric polarization in individual live cells varied during N → P modulation and remained constant during P → N modulation.

To confirm those findings, we statistically derived a Gaussian distribution function from the histogram data (Figure 3a) and derived reliable crossover frequency ($f_{co}$) values from the average values of the functions with each standard deviation (Figure 3b). The $f_{co}$ of the N → P modulation started to increase along with the FSR, whereas the $f_{co}$ of the P → N modulation remained steady at every FSR, producing discrepancies in $f_{co}$ with N → P and P → N modulations. Because $f_{co}$ represents the frequency at which the polarization


https://dx.doi.org/10.1021/acs.jpclett.0c01427
J. Phys. Chem. Lett. 2020, 11, 7197−7203

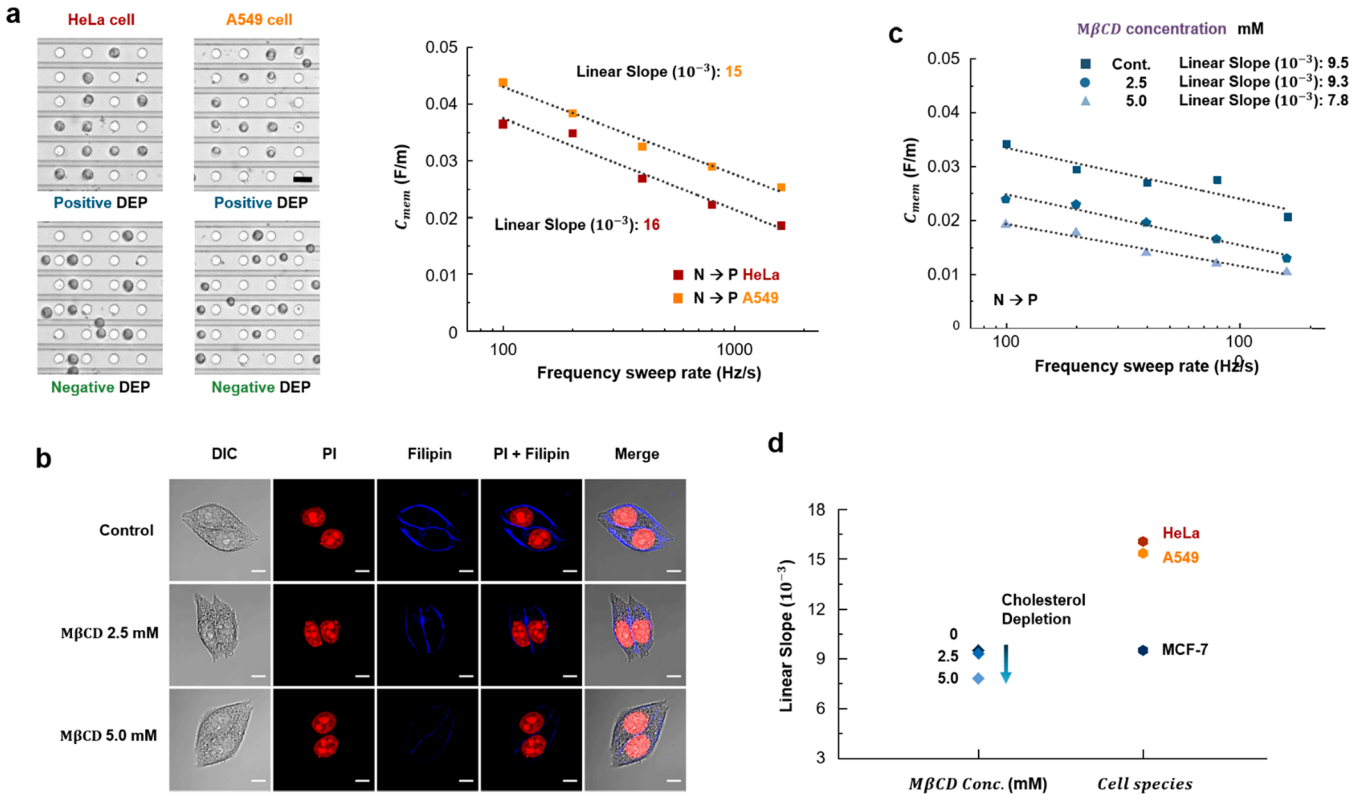


**Figure 4.** Variable capacitance of HeLa, A549 cells, and cholesterol-depleted MCF-7 cells. (a) Variable capacitance of HeLa cells and A549 cells (measurement results in Supporting Information S13), scale bar 30 $\mu$m. (b) Confocal microscope images of cholesterol-depleted MCF-7 cells at three concentrations of M$\beta$CD: 0, 2.5, and 5.0 mM. Scale bar, 10 $\mu$m (Supporting Information S11). (c) Variable capacitances at different M$\beta$CD concentrations during N → P modulation. (d) Linear slope of the variable capacitances of different cell types and M$\beta$CD concentrations during N → P modulation.

of a cellular membrane is equivalent to that of the medium surrounding it,[21] the discrepancies indicate that differences occur in that equivalent state depending on the two distinct frequency modulations. The polarization denotes the charge displacement generated by residual free charges at the dielectric boundaries (e.g., the cell membrane and surrounding medium)[23] under an alternating current. The charges that accumulate on the inner membrane surface, which respond to the ions from the surrounding medium that accumulate on the outer cell surface, are reversed at each half-cycle of the AC electric field.[24] During N → P modulation, the charge displacement inside the cellular membrane starts to increase along with the frequency (i.e., 1 kHz → 41 kHz, as shown in Figure 1c) until it reaches a balanced state at $f_{co}$. Because the incremental charge displacement does not occur instantaneously, it takes time to approach the steady-state level.[21] However, the charge displacement outside the cellular membrane starts to increase as the frequency decreases (i.e., 41 kHz → 1 kHz) during P → N modulation, and the displacement process is much faster than that inside the cellular membrane.[21,25,26] Therefore, when the FSR is increased (i.e., 100 Hz/s → 1600 Hz/s) during the N → P modulation, the times to reach the balanced state were delayed, resulting in the increase of the $f_{co\text{-}effetive}$ for the balanced state, whereas they produced no delay as increasing the FSR during the P → N modulation, resulting in being stayed at the $f_{co\text{-}effective}$ for the balanced state. Therefore, the different characteristics shown in Figures 3b are identified: the dielectric polarizations of individual live cells are a function of the frequency modulation direction and sweep rate. Moreover, $f_{co}$ can be converted into a membrane capacitance. Figures 3c show the results of that conversion, where the absolute value of the linear slope of the variable capacitance responding to variable dielectric polarizations is $9.5 \times 10^{-3}$ during N → P modulation and approximately constant during P → N modulation. For the further discussion of variation in cellular dielectric polarizations, we focus on the variable capacitance results during N → P modulation.

When we repeated the experiments with different cell types (HeLa and A549), we found the same characteristics in the variable capacitance of the cellular membrane dielectric polarization response to an external AC electrical signal, which suggests a universality of this effect in cell membranes (Figures 4a). We also tested the variable capacitance of MCF-7 cell membranes that had been depleted of cholesterol using methyl-$\beta$-cyclodextrin (M$\beta$CD) since cholesterol plays critical roles in the maintenance of membrane permeability by increasing membrane packing and the depletion of cholesterol induces the variation of the membrane permeability, expecting the change of a ion exchange activity and the gap junction as a solute transporter. As the cholesterol was depleted (Supporting Information S10), the membrane composition changed, as shown in Figure 4b. Those composition changes increase the membrane permeability and reduced the membrane surface, allowing ions to pass easily through the membrane (Supporting Information S12).[27−29] Therefore, the value of membrane capacitances in the same FSR ranges decreased as cholesterol depletion increased, as shown in Figure 4c. More interestingly, the linear slopes of the variable capacitances decreased as a function of FSR, indicating that changes in the membrane


https://dx.doi.org/10.1021/acs.jpclett.0c01427
J. Phys. Chem. Lett. 2020, 11, 7197−7203

composition affect the dielectric polarization response to an external electrical signal. The variation in the linear slopes was also observed when testing different cell types, as shown in Figures 3c and 4a,c. Clearer pictures of those variations are summarized Figure 4d, which suggests that the variation in the linear slopes correlates strongly with the cellular membrane composition, which produces different cellular functionalities.

In conclusion, we developed a novel method for probing the dielectric polarization characteristic in the membranes of individual live cells by measuring the effective crossover frequencies, $f_{\text{co-effective,}}$ using MDFS. Under the method, we simultaneously measured $f_{\text{co-effective}}$ of numerous individual MCF-7 cells under the exact same environment in both the direction and rate of frequency modulation of an external electrical signal. We also extracted statistically reliable average crossover frequency, $f_{\text{co}}$, using a Gaussian fit of the measured $f_{\text{co-effective}}$ of MCF-7 cells, and found that $f_{\text{co}}$, live MCF-7 cells differed with change in both the direction and rate of frequency modulation, which indicates that the dielectric polarization property of live MCF-7 cells was varied. This variable dielectric polarization characteristic was also observed in different cell types such as HeLa and A549 cells. In addition, the variable membrane capacitance, which is involved in the variable dielectric polarization characteristic, was induced by the $f_{\text{co}}$ of such cells. More importantly, we demonstrated that the variable capacitance across the membranes of live cells can be adjusted by regulating the membrane composition. This is the first reported evidence that the dielectric polarization characteristic within the membranes of individual live cells varies with respect to the change of the external stimulations. The finding could be used to investigate the cellular membrane functionalities involved in dielectric polarization properties of live cells including regulation of ion channel, membrane transports, pumps, and the transmembrane ion flow generated by neuronal potential, which is correlated to the regulation of cell membrane capacitance in FSR system,[1−4,30] and those results could be used to develop biological circuits, such as neuronal devices, biomaterial semiconductor electronic circuits, or mammalian memory devices.[31−33]

## EXPERIMENTAL METHODS

*Sample Preparation.* The MCF-7 human breast-cancer cell line (ATCC, Manassas, VA, USA) was grown in Dulbecco's Modified Eagle's Medium (Lonza, Walkersville, MD, USA) supplemented with 10% fetal bovine serum (FBS) and 1% penicillin-streptomycin (Gibco, Grand Island, NY, USA) and incubated at 37 °C in a humidified atmosphere with 5% $CO_2$. For the experiments, MCF-7 cells were seeded into six-well plates at $2 \times 10^5$ cells/well in buffer solution and incubated for 48 h. After that, the cells were detached by treatment with 0.25% trypsin/EDTA and washed three times with DEP buffer solution containing 8.6% (w/w) sucrose, 0.3% (w/w) glucose, and 1.0 mg/mL bovine serum albumin (BSA). Subsequently, they were resuspended in 1 mL of DEP buffer at a concentration of ∼100 cells/$\mu$L. The DEP buffer contained BSA to block nonspecific adhesion between cells.[34]

*Experimental Procedure Using Microfluidic DEP Force Spectroscopy.* A PDMS (polydimethylsiloxane) reservoir for storing the experimental solution was placed on the microfluidic device. Next, 20 $\mu$L of buffer containing suspended cells was dropped into the reservoir, and a cover glass was placed over the buffer to isolate the solution containing the cells. Then, an AC signal (2 $V_{\text{peak-peak}}$) was applied to the chrome electrodes on the chip with frequencies ranging from 1 to 41 kHz (Figure 1d), which were suitable values for manipulating the cells with positive and negative DEP forces while minimizing electrothermal effects, where the cell viability and measured data consistency of applied AC signal describes in Supporting Information S3 and S16. The frequency was varied sequentially in five phases: (1) constant 1 kHz for 100 s, (2) linear increase from 1 to 41 kHz (N → P modulation) at a chosen sweep rate, (3) constant 41 kHz for 100 s, (4) linear decrease from 41 to 1 kHz (P → N modulation) at the same sweep rate, and (5) maintenance at 1 kHz for 100 s. Those five phases compose one set of experiments, and each set was conducted using five different FSRs for the N → P and P → N modulations to provide different external energy rates: 100, 200, 400, 800, and 1600 Hz/s. All the variables of the applied signal were controlled by a LabVIEW-based (National Instruments, Austin, TX, USA) automated DEP system (Supporting Information, S2) and were verified with an oscilloscope (Wavesurfer 432, LeCroy, Chestnut Ridge, NY, USA). The automated DEP system consists of a force-spectroscopy module, an input module, and a measurement module. The force spectroscopy module contains a fabricated microfluidic DEP chip. The input module is an arbitrary function generator that applied the AC voltage signal to the DEP chip electrodes to generate DEP force. The measurement module contains an oscilloscope to measure the amplitude and phase of the applied voltage. Cellular displacements were recorded using an optical microscope (PS-888, Seiwa Optical Industrial Co., Tokyo, Japan) connected to a high-speed CCD (charge coupled device) camera (Motion Scope M3, Integrated Design Tools, Inc., Tallahassee, FL, USA) for image acquisition. The image capture rate during the stationary phases (1, 3, and 5) of the protocol was 1 frame per second. In the forward and reverse frequency regions, the capture rates were 20 frames per second for all the FSRs, with a minimum resolution of 80 Hz/frame. The synchronization and resolution of each module in quantitatively measuring the DEP-induced motion of particles were verified in our previous work.[35]

*Method for Converting $f_{co}$ to Membrane Capacitance.* By assuming that a cell membrane has very low membrane conductivity, the membrane capacitance is given by the following simple expression:

$$C_{\text{mem}} = \frac{\sigma_{\text{m}}}{\pi\sqrt{2} f_{\text{co}} r} \tag{1}$$

where $C_{\text{mem}}$, $\sigma_{\text{m}}$, and $f_{\text{co}}$ are membrane capacitance, medium conductivity, and crossover frequency, respectively (more detail is provided in Supporting Information S8).[18,36,37] Assigning the value of the measured medium conductivity (60 $\mu$S/cm) and the radius of the cell lines (9.25 $\mu$m for MCF-7, 7.48 $\mu$m for A549, 8.49 $\mu$m for HeLa, Supporting Information S9) used in our experimental setup, we present the values of the membrane capacitance according to the FSR in Figures 3c.

## ASSOCIATED CONTENT

### Supporting Information

The Supporting Information is available free of charge at https://pubs.acs.org/doi/10.1021/acs.jpclett.0c01427.

S1, fabrication of the microfluidic DEP chip; S2, automated system for controlling the frequency sweep rate and direction of microfluidic DEP force spectros-



https://dx.doi.org/10.1021/acs.jpclett.0c01427
J. Phys. Chem. Lett. 2020, 11, 7197−7203

copy; S3, cell viability before and after DEP experiments; S4, numerical analysis of DEP force using the finite-element method (FEM); S5, DEP model and Clausius–Mossotti (CM) factor of the cell; S6, programmable methods for measuring $f_{co\text{-}effective}$; S7, measurement of $f_{co\text{-}effective}$ and the determination of $f_{co}$; S8, conversion formula for membrane capacitance from crossover frequency; S9, measurement of cell radius; S10, membrane cholesterol depletion; S11, confocal microscopy; S12, intracellular $Ca^{2+}$ levels of MCF-7 treated with M$\beta$CD; S13, measured $f_{co\text{-}effective}$ for other cell types and cholesterol-depleted MCF-7 cells; S14, statistical reliability between data at various FSR conditions; S15, Joule heating in microfluidic DEP force spectroscopy system; S16, measured $f_{co\text{-}effective}$ of MCF-7 cells with different applied voltages; S17, measurement consistency of the $f_{co\text{-}effective}$ for MCF-7 cells during N → P and P → N modulation (PDF)

Time-lapsed images of DEP-driven movement of five MCF-7 cells, which is randomly chosen with experiencing forward and reverse directions of frequency sweeps (MP4)

Time-lapsed images of DEP-driven movement of MCF-7, HeLa, and A549 cells with forward and reverse directions and the sweep rate of the frequency (MP4)

Time-lapsed images of DEP-driven movement of cholesterol-depleted MCF-7 cells with forward and reverse directions and the sweep rate of the frequency (MP4)

## AUTHOR INFORMATION


### Corresponding Authors

**Sei Young Lee** − *Department of Biomedical Engineering, Yonsei University, Wonju 26493, Korea*; Email: syl235@yonsei.ac.kr

**Sang Woo Lee** − *Department of Biomedical Engineering, Yonsei University, Wonju 26493, Korea*; orcid.org/0000-0003-4633-2943; Email: yusuklee@yonsei.ac.kr

### Authors

**Insu Park** − *Holonyak Micro and Nanotechnology Laboratory, University of Illinois at Urbana—Champaign, Urbana, Illinois 61801, United States*

**Jong Won Lim** − *Department of Biomedical Engineering, Yonsei University, Wonju 26493, Korea*

**Sung Hoon Kim** − *Department of Biomedical Laboratory Science, Yonsei University, Wonju 26493, Korea; Department of Biomedical Laboratory Science, Korea Nazarene University, Chungnam 31172, Korea*

**Seungyeop Choi** − *Department of Biomedical Engineering, Yonsei University, Wonju 26493, Korea*; orcid.org/0000-0002-3192-579X

**Kwan Hwi Ko** − *Department of Biomedical Engineering, Yonsei University, Wonju 26493, Korea*

**Myung Gu Son** − *Department of Biomedical Engineering, Yonsei University, Wonju 26493, Korea*

**Woo-Jin Chang** − *Mechanical Engineering Department, University of Wisconsin—Milwaukee, Milwaukee, Wisconsin 53211, United States*

**Young Ro Yoon** − *Department of Biomedical Engineering, Yonsei University, Wonju 26493, Korea*

**Sejung Yang** − *Department of Biomedical Engineering, Yonsei University, Wonju 26493, Korea*

**Jaehong Key** − *Department of Biomedical Engineering, Yonsei University, Wonju 26493, Korea*

**Yoon Suk Kim** − *Department of Biomedical Laboratory Science, Yonsei University, Wonju 26493, Korea*

**Kilho Eom** − *Biomechanics Laboratory, College of Sport Science, Sungkyunkwan University, Suwon 16419, Korea*

**Rashid Bashir** − *Holonyak Micro and Nanotechnology Laboratory and Department of Bioengineering, University of Illinois at Urbana—Champaign, Urbana, Illinois 61801, United States; Carle Illinois College of Medicine, Urbana, Illinois 61801, United States; Mayo-Illinois Alliance for Technology Based Healthcare, Urbana, Illinois 61801, United States*

Complete contact information is available at: https://pubs.acs.org/10.1021/acs.jpclett.0c01427

### Author Contributions

[@]I.P., J.W.L., and S.H.K. contributed equally.


### Notes

The authors declare no competing financial interest.

## ACKNOWLEDGMENTS

This work was supported by National Research Foundation of Korea (NRF) grants (NRF-2017R1A2B2002076 and NRF-2016R1D1A1A02937019) and Brain Korea 21 Plus project (S20SR41D0101) funded by the Korean government.

## REFERENCES


(1) Spira, M. E.; Hai, A. Multi-electrode array technologies for neuroscience and cardiology. *Nat. Nanotechnol.* **2013**, *8*, 83−94.

(2) Howell, B.; Medina, L. E.; Grill, W. M. Effects of frequency-dependent membrane capacitance on neural excitability. *J. Neural Eng.* **2015**, *12*, 056015.

(3) Melcr, J.; Bonhenry, D.; Timr, S.; Jungwirth, P. Transmembrane potential modeling: comparison between methods of constant electric field and ion imbalance. *J. Chem. Theory Comput.* **2016**, *12*, 2418−2425.

(4) Bezanilla, F. How membrane proteins sense voltage. *Nat. Rev. Mol. Cell Biol.* **2008**, *9*, 323−332.

(5) Carrillo, L.; Cucu, B.; Bandmann, V.; Homann, U.; Hertel, B.; Hillmer, S.; Thiel, G.; Bertl, A. High-resolution membrane capacitance measurements for studying endocytosis and exocytosis in yeast. *Traffic* **2015**, *16*, 760−772.

(6) Robinson, J. T.; Jorgolli, M.; Shalek, A. K.; Yoon, M. H.; Gertner, R. S.; Park, H. Vertical nanowire electrode arrays as a scalable platform for intracellular interfacing to neuronal circuits *Nat. Nat. Nanotechnol.* **2012**, *7*, 180−184.

(7) Lin, Z. C.; Xie, C.; Osakada, Y.; Cui, Y.; Cui, B. Iridium oxide nanotube electrodes for sensitive and prolonged intracellular measurement of action potentials. *Nat. Commun.* **2014**, *5*, 3206.

(8) Tian, B.; Cohen-Karni, T.; Qing, Q.; Duan, X.; Xie, P.; Lieber, C. M. Three-dimensional, flexible nanoscale field-effect transistors as localized bioprobes. *Science* **2010**, *329*, 830−834.

(9) Garten, M.; Mosgaard, L. D.; Bornschlögl, T.; Dieudonné, S.; Bassereau, P.; Toombes, G. E. Whole-GUV patch-clamping. *Proc. Natl. Acad. Sci. U. S. A.* **2017**, *114*, 328−333.

(10) Pui, T. S.; Sudibya, H. G.; Luan, X.; Zhang, Q.; Ye, F.; Huang, Y.; Chen, P. Non-invasive Detection of Cellular Bioelectricity Based on Carbon Nanotube Devices for High-Throughput Drug Screening. *Adv. Mater.* **2010**, *22*, 3199−3203.

(11) Pethig, R. Dielectrophoresis: using inhomogeneous AC electrical fields to separate and manipulate cells. *Crit. Rev. Biotechnol.* **1996**, *16*, 331−348.

(12) Adams, T. N. G.; Leonard, K. M.; Minerick, A. R. Frequency sweep rate dependence on the dielectrophoretic response of

polystyrene beads and red blood cells. *Biomicrofluidics* **2013**, *7*, No. 064114.
(13) Choi, S.; Ko, K.; Lim, J.; Kim, S. H.; Woo, S. H.; Kim, Y. S.; Key, J.; Lee, S. Y.; Park, I. S.; Lee, S. W. Non-Linear Cellular Dielectrophoretic Behavior Characterization Using Dielectrophoretic Tweezers-Based Force Spectroscopy inside a Microfluidic Device. *Sensors* **2018**, *18* (10), 3543.
(14) Park, I. S.; Eom, K.; Son, J.; Chang, W. J.; Park, K.; Kwon, T.; Yoon, D. S.; Bashir, R.; Lee, S. W. Microfluidic multifunctional probe array dielectrophoretic force spectroscopy with wide loading rates. *ACS Nano* **2012**, *6*, 8665−8673.
(15) Park, I. S.; Kwak, T. J.; Lee, G.; Son, M.; Choi, J. W.; Choi, S.; Nam, K.; Lee, S.; Chang, W.; Eom, K.; Yoon, D. S.; Lee, S.; Bashir, R.; Lee, S. W. Biaxial dielectrophoresis force spectroscopy: A stoichiometric approach for examining intermolecular weak binding interactions. *ACS Nano* **2016**, *10* (4), 4011−4019.
(16) Choi, S.; Lee, G.; Park, I. S.; Son, M.; Kim, W.; Lee, H.; Lee, S.; Na, S.; Yoon, D. S.; Bashir, R.; Park, J.; Lee, S. W. Detection of silver ions using dielectrophoretic tweezers-based force spectroscopy. *Anal. Chem.* **2016**, *88*, 10867−10875.
(17) Park, I. S.; Lee, J.; Lee, G.; Nam, K.; Lee, T.; Chang, W. J.; Kim, H.; Lee, S.; Seo, J.; Yoon, D. S.; Lee, S. W. Real-time analysis of cellular response to small-molecule drugs within a microfluidic dielectrophoresis device. *Anal. Chem.* **2015**, *87*, 5914−5920.
(18) Salmanzadeh, A.; Sano, M. B.; Gallo-Villanueva, R. C.; Roberts, P. C.; Schmelz, E. M.; Davalos, R. V. Investigating dielectric properties of different stages of syngeneic murine ovarian cancer cells. *Biomicrofluidics* **2013**, *7*, No. 011809.
(19) Jung, Y. J.; Lee, T.; Choi, S.; Lee, S. Y.; Key, J.; Yoo, Y. M.; Chang, W.; Kim, H.; Lee, S. W. Selective position of individual cells without lysis on a circular window array using dielectrophoresis in a microfluidic device. *Microfluid. Nanofluid.* **2017**, *21*, 150.
(20) Lee, A. V.; Oesterreich, S.; Davidson, N. E. MCF-7 cells-changing the course of breast cancer research and care for 45 years. *JNCI J. Natl. Cancer Inst.* **2015**, *107*, djv073.
(21) Pethig, R. R. *Dielectrophoresis: Theory, methodology and biological applications*; John Wiley & Sons, 2017.
(22) Jones, T. B. *Electromechanics of particles*; Cambridge University Press, 2005.
(23) Desmond, M.; Mavrogiannis, N.; Gagnon, Z. Maxwell-Wagner polarization and frequency-dependent injection at aqueous electrical interfaces. *Phys. Rev. Lett.* **2012**, *109*, 187602.
(24) Minerick, A. R.; Zhou, R.; Takhistov, P.; Chang, H. C. Manipulation and characterization of red blood cells with alternating current fields in microdevices. *Electrophoresis* **2003**, *24*, 3703−3717.
(25) Tait, M. J.; Suggett, A.; Franks, F.; Ablett, S.; Quickenden, P. A. Hydration of monosaccharides: A study by dielectric and nuclear magnetic relaxation. *J. Solution Chem.* **1972**, *1*, 131−151.
(26) Ellison, W. J.; Lamkaouchi, K.; Moreau, J. M. Water: A dielectric reference. *J. Mol. Liq.* **1996**, *68*, 171−279.
(27) Beseničar, M. P.; Bavdek, A.; Kladnik, A.; Maček, P.; Anderluh, G. Kinetics of cholesterol extraction from lipid membranes by methyl-β-cyclodextrin-A surface plasmon resonance approach. *Biochim. Biophys. Acta, Biomembr.* **2008**, *1778*, 175−184.
(28) Lam, R. S.; Shaw, A. R.; Duszyk, M. Membrane cholesterol content modulates activation of BK channels in colonic epithelia. *Biochim. Biophys. Acta, Biomembr.* **2004**, *1667*, 241−248.
(29) Shmygol, A.; Noble, K.; Wray, S. Depletion of membrane cholesterol eliminates the Ca2+-activated component of outward potassium current and decreases membrane capacitance in rat uterine myocytes. *J. Physiol.* **2007**, *581*, 445−456.
(30) Brown, M. S.; Goldstein, J. L. A proteolytic pathway that controls the cholesterol content of membranes, cells, and blood. *Proc. Natl. Acad. Sci. U. S. A.* **1999**, *96*, 11041−11048.
(31) Kalita, H.; Krishnaprasad, A.; Choudhary, N.; Das, S.; Dev, D.; Ding, Y.; Tethard, L.; Chung, H.; Jung, Y.; Roy, T. Artificial Neuron using Vertical MoS 2/Graphene Threshold Switching Memristors. *Sci. Rep.* **2019**, *9*, 53.
(32) Bettinger, C. J.; Bao, Z. Biomaterials-based organic electronic devices. *Polym. Int.* **2010**, *59*, 563−567.
(33) Tigges, M.; Marquez-Lago, T. T.; Stelling, J.; Fussenegger, M. A tunable synthetic mammalian oscillator. *Nature* **2009**, *457*, 309−312.
(34) Kobayashi, M.; Kim, S. H.; Nakamura, H.; Kaneda, S.; Fujii, T. Cancer cell analyses at the single cell-level using electroactive microwell array device. *PLoS One* **2015**, *10*, No. e0139980.
(35) Kim, M. H.; Lee, J.; Nam, K.; Park, I. S.; Son, M.; Ko, H.; Lee, S.; Yoon, D. S.; Chang, W.; Lee, S. Y.; Yoon, Y. R.; Lee, S. W. Automated Dielectrophoretic Tweezers-Based Force Spectroscopy System in a Microfluidic Device. *Sensors* **2017**, *17*, 2272.
(36) Chan, K. L.; Morgan, H.; Morgan, E.; Cameron, I. T.; Thomas, M. R. Measurements of the dielectric properties of peripheral blood mononuclear cells and trophoblast cells using AC electrokinetic techniques. *Biochim. Biophys. Acta, Mol. Basis Dis.* **2000**, *1500*, 313−322.
(37) Williams, S. K. R.; Caldwell, K. D. *Field-flow fractionation in biopolymer analysis*; Springer Science & Business Media, 2011.


https://dx.doi.org/10.1021/acs.jpclett.0c01427
J. Phys. Chem. Lett. 2020, 11, 7197−7203